Research article JHEP|Reports

Molecular magnetic resonance imaging of liver inflammation using an oxidatively activated probe

Authors

Veronica Clavijo Jordan, Mozhdeh Sojoodi, Stuti Shroff, Patricia Gonzalez Pagan, Stephen Cole Barrett, Jeremy Wellen, Kenneth K. Tanabe, Raymond T. Chung, Peter Caravan, Eric M. Gale

Correspondence

emgale@mgh.harvard.edu (E.M. Gale).

Graphical abstract

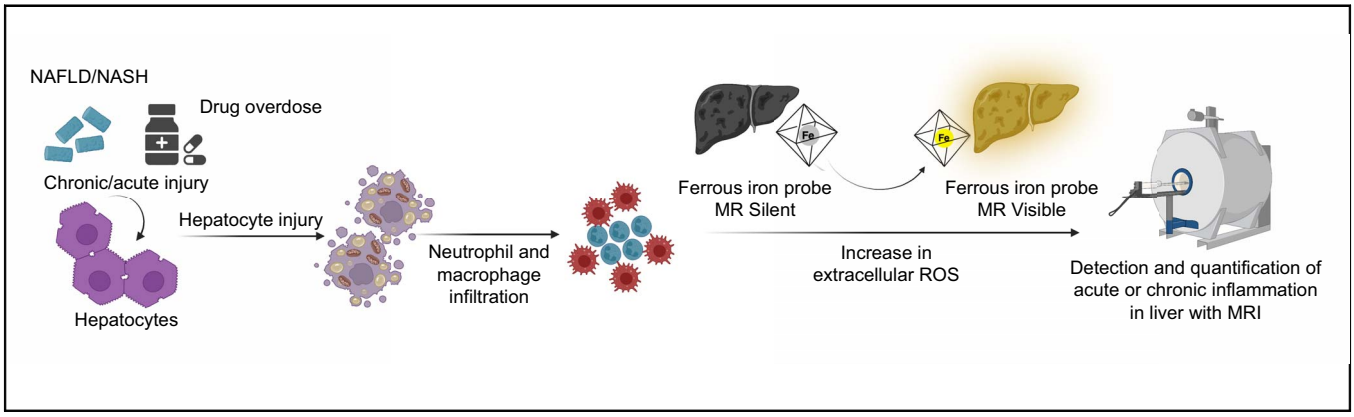

Highlights

- New MR imaging probe switches from 'off' to 'on' in the presence of liver inflammation.
- Imaging distinguishes NASH from non-NASH in mice.
- Imaging correlates with inflammatory change in mouse model of liver injury.

Impact and implications

Non-invasive tests to diagnose and measure liver inflammation are underdeveloped. Inflammatory cells such as neutrophils release reactive oxygen species which creates an inflammatory liver microenvironment that can drive chemical oxidation. We recently invented a new class of magnetic resonance imaging probe that is made visible to the scanner only after chemical oxidation. Here, we demonstrate how this imaging technology could be applied as a non-invasive biomarker for liver inflammation.

https://doi.org/10.1016/j.jhepr.2023.100850

Research article

JHEP|Reports

Molecular magnetic resonance imaging of liver inflammation using an oxidatively activated probe

Veronica Clavijo Jordan,[1,2,†] **Mozhdeh Sojoodi**,[2,3,†] Stuti Shroff,[2,4] Patricia Gonzalez Pagan,[1,2] Stephen Cole Barrett,[2,3] Jeremy Wellen,[5] Kenneth K. Tanabe,[2,3] Raymond T. Chung,[2,6] Peter Caravan,[1,2] Eric M. Gale[1,2,*]

[1]*Athinoula A. Martinos Center for Biomedical Imaging, The Institute for Innovation in Imaging, Department of Radiology, Massachusetts General Hospital, Boston, MA, USA;* [2]*Harvard Medical School, Boston, MA, USA;* [3]*Division of Gastrointestinal and Oncologic Surgery, Massachusetts General Hospital, Boston, MA, USA;* [4]*Department of Pathology, Massachusetts General Hospital, Boston, MA, USA;* [5]*Bristol Meyers Squibb, Cambridge, MA, USA;* [6]*Gastroenterology Unit, Department of Medicine, Massachusetts General Hospital, Boston, MA, USA*

JHEP Reports **2023.** https://doi.org/10.1016/j.jhepr.2023.100850

Background & Aims: Many liver diseases are driven by inflammation, but imaging to non-invasively diagnose and quantify liver inflammation has been underdeveloped. The inflammatory liver microenvironment is aberrantly oxidising owing in part to reactive oxygen species generated by myeloid leucocytes. We hypothesised that magnetic resonance imaging using the oxidatively activated probe Fe-PyC3A will provide a non-invasive biomarker of liver inflammation.

Methods: A mouse model of drug-induced liver injury was generated through intraperitoneal injection of a hepatoxic dose of acetaminophen. A mouse model of steatohepatitis was generated via a choline-deficient, L-amino acid defined high-fat diet (CDAHFD). Images were acquired dynamically before and after intravenous injection of Fe-PyC3A. The contrast agent gadoterate meglumine was used as a non-oxidatively activated negative control probe in mice fed CDAHFD. The (post-pre) Fe-PyC3A injection change in liver *vs.* muscle contrast-to-noise ratio (ΔCNR) recorded 2 min post-injection was correlated with liver function test values, histologic scoring assigned using the NASH Clinical Research Network criteria, and intrahepatic myeloid leucocyte composition determined by flow cytometry.

Results: For mice receiving i.p. injections of acetaminophen, intrahepatic neutrophil composition correlated poorly with liver test values but positively and significantly with ΔCNR ($r = 0.64$, $p < 0.0001$). For mice fed CDAHFD, ΔCNR generated by Fe-PyC3A in the left lobe was significantly greater in mice meeting histologic criteria strongly associated with a diagnosis NASH compared to mice where histology was consistent with likely non-NASH ($p = 0.0001$), whereas no differential effect was observed using gadoterate meglumine. In mice fed CDAHFD, ΔCNR did not correlate strongly with fractional composition of any specific myeloid cell subpopulation as determined by flow cytometry.

Conclusions: Magnetic resonance imaging using Fe-PyC3A merits further evaluation as a non-invasive biomarker for liver inflammation.

Impact and implications: Non-invasive tests to diagnose and measure liver inflammation are underdeveloped. Inflammatory cells such as neutrophils release reactive oxygen species which creates an inflammatory liver microenvironment that can drive chemical oxidation. We recently invented a new class of magnetic resonance imaging probe that is made visible to the scanner only after chemical oxidation. Here, we demonstrate how this imaging technology could be applied as a non-invasive biomarker for liver inflammation.

Introduction

Acute and chronic liver diseases impose a major burden on global health, with liver-related mortality accounting for an estimated 3.5% of deaths worldwide.[1] There is an inflammatory component to most liver disease states, and in many cases inflammation represents a key driver of disease progression.[2,3] Inflammation is a key factor in histologic scoring of many acute and chronic liver disease states, but clinical imaging tools to non-invasively diagnose liver inflammation or characterise inflammation disease activity are underdeveloped.[4,5] Imaging probes targeted to cellular or molecular level changes that occur within the inflammatory liver microenvironment are challenging to develop, as the immunologic and excretory functions of the liver often result in non-specific probe accumulation, leading to high background signal.[6–9]

Concentrations of reactive oxygen species (ROS) are tightly regulated in normal liver, but can be upregulated substantially in inflammatory disease states.[10] During inflammation, infiltrating myeloid leucocytes secrete ROS into the extracellular spaces via

Keywords: Drug-induced liver injury; Steatohepatitis; Reactive oxygen species.
Received 19 August 2022; received in revised form 6 July 2023; accepted 10 July 2023; available online 18 July 2023

† These authors contributed equally.

* Corresponding author. Address: 149 Thirteenth Street, Suite 2301, Charlestown, MA, 02129, USA. Tel.: +1-617-726-3197; Fax: +1-617-726-7422.
E-mail address: emgale@mgh.harvard.edu (E.M. Gale).

activity of the membrane bound nicotinamide adenine dinucleotide phosphate oxidase II enzyme, generating an aberrant oxidising liver microenvironment that can result in hepatocellular injury and drive pathologic activation of hepatic stellate cells, culminating in loss of liver function and liver fibrosis.[2] In this regard, molecular imaging of liver ROS and/or oxidative changes within the extracellular spaces of the liver microenvironment offers a potentially powerful non-invasive marker for disease activity in inflammatory liver conditions.

We hypothesised that the recently reported oxidatively activated magnetic resonance (MR) imaging probe Fe-PyC3A could be used to image ROS upregulation resulting from liver inflammation. Fe-PyC3A is a low molecular weight compound that is rapidly switched from a complex of divalent iron (Fe^{2+}) to the corresponding complex of trivalent iron (Fe^{3+}) via ROS-mediated oxidation.[11] In the Fe^{2+} state, the relaxivity (a measure of MR imaging probe efficacy) of Fe-PyC3A is very low, rendering the complex a weak MR signal generator, whereas the corresponding Fe^{3+} complex possess over 10-fold greater relaxivity and behaves as a very effective MR signal generator. Fe-PyC3A is administered as the low-relaxivity Fe^{2+} complex, which is favoured in normal tissues where ROS concentrations and redox potential are tightly regulated, but converts to the high-relaxivity Fe^{3+} complex in inflamed tissue with expanded populations of ROS-releasing myeloid leucocytes.

In this study, we evaluated whether MR imaging using Fe-PyC3A is capable of detecting pathologic changes in liver myeloid leucocyte content in mouse models of drug-induced liver injury (DILI) and non-alcoholic steatohepatitis (NASH).

Materials and methods

Animal models

Animals received humane care per criteria outlined in the NIH Guide for the Care and Use of Laboratory Animals and were approved by the Massachusetts General Hospital Institutional Animal Care and Use Committee. Experiments were designed and reported in accordance with Animal Research: Reporting in Vivo Experiments (ARRIVE) guidelines.[12] DILI was generated in male C57BL/6 mice (5 weeks of age) by administering a hepatotoxic dose of acetaminophen (formulated at 15 mg/ml in saline) intraperitoneally. Mice received either 300 mg/kg acetaminophen (N = 9), 450 mg/kg acetaminophen (N = 19), or saline vehicle (N = 12). The 300 mg/kg and 450 mg/kg acetaminophen doses required injection volumes of 0.5 ml and 0.75 ml, respectively. For vehicle-treated mice, 0.5 ml saline was injected to N = 2 and 0.75 ml saline injected to N = 10 mice. Imaging was performed between 16 and 22 h after i.p. injections. Imaging and flow cytometry data exhibited substantial variability within these groups. For comparisons, group sizes of N = 9 provide 80% power to detect a 300% difference in mean liver signal enhancement or intrahepatic myeloid cell content, assuming a relative standard deviation of 80% and alpha = 0.05. To induce steatohepatitis, L-amino acid diet with 60 kcal% fat with 0.1% added methionine and no added choline (*i.e.* choline deficient, high-fat diet, or CDAHFD)[13] purchased from Research Diets (New Brunswick, NJ, USA) was administered to male C57BL/6 mice starting at 5 weeks of age. For experiments to evaluate Fe-PyC3A imaging in the context of histologic scoring, mice were imaged following regimens of CDAHFD lasting either 2 days (N = 4), 5 days (N = 3), 7 days (N = 4), or 13 days (N = 2). A group of age-matched mice receiving normal diet were also imaged (N = 3). Study of mice on CDAHFD ranging between 0 (normal diet) to 13 days of nutritional NAFLD induction enabled imaging of the non-alcoholic fatty liver disease (NAFLD) activity score (NAS) ranging 0–7 and 0–8 within the left and right lobes, respectively. These mice yielded groups of N = 9 left-lobe specimens that scored NAS ≤3 and N = 5 that scored NAS ≥5 (see Materials and methods: *Ex vivo* tissue analysis). For experiments to correlate Fe-PyC3A imaging with intrahepatic myeloid cell content determined using flow cytometry, age-matched mice were imaged 4 weeks (N = 5 CDAHFD, N = 4 normal diet), 6 weeks (N = 6 CDAHFD, N = 4 normal diet), and 8 weeks (N =6 CDAHFD, N = 4 normal diet) after diet was initiated. Because no significant differences were observed for mice fed between 4 and 8 weeks normal diet, the mice were treated as a single group of N = 12. Intrahepatic macrophage composition changes substantially between 4 and 8 weeks after nutritional NAFLD induction, and imaging within this window enabled us to better examine correlations between Fe-PyC3A liver enhancement and myeloid cell subpopulations. For comparisons between mice receiving CDAHFD, group sizes of N = 5 provide 80% power to detect 200% difference in mean values, assuming a relative standard deviation of 50% and alpha = 0.05. Each mouse was euthanised after imaging. A total of 86 mice were used in this study.

Imaging probes

Fe-PyC3A is the iron complex of *N*-picolyl-*N*,*N*′,*N*′-*trans*-1,2-cyclohexyleneiaminetriacetic acid. The relaxivity, r_1, values of Fe-PyC3A in the Fe^{2+} and Fe^{3+} oxidation states are 0.18 mM^{-1} s^{-1} and 2.4 mM^{-1} s^{-1} at 4.7T and room temperature, respectively.[11] Fe-PyC3A was isolated in the low-relaxivity Fe^{2+} state and formulated in water at a concentration of 100 mM. Gadoterate meglumine (Gd-DOTA) is an extracellular fluid MRI contrast agent market by Guerbet. Gd-DOTA was formulated at 100 mM.

Magnetic resonance imaging and analysis

Mice were imaged with a 4.7T small bore scanner (Bruker Biospec) with a custom-built volume coil. To deliver Fe-PyC3A intravenously, the mouse tail vein was cannulated while sedated via a nose cone-delivered mixture of isoflurane and oxygen (1–2% iso), and sedation was maintained during the MR imaging protocol. Animals were dynamically imaged by repeating a coronal multi-slice 2D T_1-weighted gradient echo sequence (echo time [TE]/repetition time [TR]= 2.9/190.4 ms, flip angle [FA] = 60°, matrix = 140 × 140, field of view = 33 mm × 33 mm, slice thickness = 1 mm, acquisition time = 104 s) before and up to 25 min after injection of 0.2 mmol/kg Fe-PyC3A (2 μl solution per gram body weight) via tail vein injection. For mice fed CDAHFD or normal diet, a six-point multiple gradient echo (MGE) Dixon scan to quantify liver fat fraction was also acquired before Fe-PyC3A injection (TE = 1.46, 2.19, 2.92, 3.65, 4.38, 5.11, TR = 140 ms, FA = 15°, matrix = 128 × 128, field of view: 33 mm × 33 mm, slice thickness = 1 mm, slices = 15). Fat fraction was obtained with Matlab (Mathworks, Natick, MA, USA) using the Dixon 3 in-phase and 3 out-of-phase images, an iterative least squares estimation method, and T_2* correction modelling.[14,15] For mice imaged between 0 and 13 days after CDAHFD injection, 0.1 mmol/kg Gd-DOTA (1 μl per gram body weight) was injected 30 min after Fe-PyC3A, at which point liver signal enhancement did not differ significantly from pre-injection levels.

MR images were analysed with the ImageJ and Horos software. Regions of interest (ROI) were drawn in the left and right liver lobes, back muscle, and air outside of the animal. Liver *vs.*

muscle contrast-to-noise ratios (CNRs) were computed using the following formula, where SI corresponds to mean signal intensity in the ROI and noise is defined as the standard deviation of the signal in the ROI drawn in the air outside of the animal.

$$CNR = \frac{(SI_{liver} - SI_{muscle})}{noise}$$

The magnitude of Fe-PyC3A related liver enhancement was expressed as the (post-pre)injection change in liver *vs*. muscle CNR (ΔCNR).

Serum liver test analysis

Serum was harvested from subsets of mice receiving i.p. injections of vehicle (N = 6) or 450 mg/kg acetaminophen (N = 11) immediately after euthanasia. Serum was submitted to the MGH Center for Comparative Medicine Core for quantification of liver function markers.

Ex vivo tissue analysis

Liver tissue from representative subsets of mice receiving i.p. injections of vehicle and with normal liver function tests (N = 4) or with acetaminophen and with alanine aminotransferase (ALT) elevated five-fold or more above the normal upper limit (N = 8) were stained with haematoxylin and eosin stain (H&E) for histological analysis including signs of necrosis and inflammation. For mice studied in the context of NASH imaging, H&E stained specimens were analysed in a blinded manner and graded for steatosis (0–3), lobular inflammation (0–3) and hepatocellular ballooning (0–2) according to the NASH Clinical Research Network (CRN) criteria,[16] and a semi-quantitative NAS (range 0–8) was determined from the unweighted sum of these values. NAS ≥5 is associated with a likelihood of NASH, whereas NASH is unlikely in NAS ≤3. Specimens receiving NAS ≥5, NAS ≤3, and NAS = 4 were grouped as 'likely NASH', 'likely non-NASH', and 'borderline', respectively. Sirius Red staining was used to stage fibrosis. Details of flow cytometry and myeloperoxidase immunostaining are described in the Supplementary information (Fig. S1).

Statistics

Comparisons of serum liver tests in mice treated with vehicle and acetaminophen and of ΔCNR_{2m} recorded in mice with NAS corresponding to likely non-NASH and likely NASH were made by a two-sided unpaired *t* test. Comparisons of intrahepatic myeloid cell sub-populations and of ΔCNR_{2m} between groups receiving vehicle, 300 mg/kg, and 450 mg/kg acetaminophen, or between groups fed normal diet and 4-, 6-, and 8-week regimens of CDAHFD were made by one-way ANOVA followed by Tukey's *post-hoc* test for multiple comparisons. Correlations were determined by calculating the Pearson's product moment correlation coefficient, significance was determined using a two-tailed test. Values recorded in the right and left liver lobes were analysed independently. For all comparisons and correlations $p < 0.05$ was considered significant.

Results

Molecular MR imaging of liver inflammation in a mouse model of DILI

To investigate whether MR imaging using Fe-PyC3A was capable of detecting liver inflammatory changes associated with DILI, mice were imaged between 16 and 22 h after i.p administration of a hepatotoxic dose of either 300 mg/kg or 450 mg/kg acetaminophen, or saline vehicle as control. Based on the previously studied pharmacokinetics of the isostructural compound Mn-PyC3A,[17–20] i.v. administration of Fe-PyC3A is expected to rapidly distribute through the liver extracellular spaces, and then clear within minutes partially through hepatocellular uptake. We thus hypothesised that MR imaging data acquired at early time points consistent with predominantly extracellular liver distribution of Fe-PyC3A would be most sensitive to the presence of ROS-releasing myeloid cells. In this regard, MR imaging 2 min after Fe-PyC3A injection (extracellular phase) and at delayed time points where substantial hepatocellular accumulation of Fe-PyC3A are anticipated were separately correlated with intrahepatic neutrophil and macrophage composition determined by flow cytometry. Serum from subsets of mice receiving either vehicle or 450 mg/kg acetaminophen was analysed to compare the specificity of MRI using Fe-PyC3A *vs*. serum liver tests to detect changes in liver inflammatory infiltrate.

Liver tests do not reflect large variations in liver inflammatory infiltrate composition

Serum levels of albumin, alkaline phosphatase (ALP), ALT, aspartate transaminase (AST), bilirubin, gamma-glutamyl transferase, total globulin, and total protein recorded from subsets of mice treated with vehicle or acetaminophen are compared in Table S1. Serum analysis identified significantly elevated levels of ALP, ALT, and AST in mice treated with acetaminophen over mice receiving vehicle (160 ± 23 U/L *vs.* 130 ± 21, $p = 0.026$ for ALP; 8,100 ± 5,900 *vs.* 150 ± 200 U/L, $p = 0.011$ for ALT; 3,700 ± 2,600 *vs.* 450 ± 710, $p = 0.0020$ U/L for AST, Fig. 1A–C, respectively). Acetaminophen overdose resulted in ALT levels greater than five-fold over the normal upper limit in every mouse analysed, consistent with DILI.[21] Liver function markers were within the normal reference range for most vehicle treated mice. Serum ALT levels above the normal upper limit were recorded for one vehicle-treated mouse, and AST levels were elevated for two, but these relatively modest increases are not consistent with DILI.[21]

H&E staining identified a necroinflammatory pattern of injury in mice receiving acetaminophen overdose, also consistent with DILI (Fig. S2). Liver parenchyma showed necrosis involving the perivenular zone 3 parenchyma with extension into zone 2. The inflammatory response involves the recruitment of neutrophils and monocytes. Marked congestion of central veins was also observed following acetaminophen overdose. Necroinflammatory changes were not observed in mice that did not receive acetaminophen.

The relative percentages of left liver lobe leucocyte composition comprising neutrophils and macrophage sub-populations after treatment with either with vehicle, 300 mg/kg, or 450 mg/kg acetaminophen are compared in Fig 1D–G and Table S2. Intrahepatic neutrophil ($CD45^+Ly6G^+$) content and M1 macrophage ($CD45^+CD11b^+F4/80^+CD11c^+$) content varied substantially within each treatment group and no significant differences were observed between groups (Fig. 1D and E). Migratory macrophage ($CD45^+CD11b^+F4/80^+CCR2^+$) composition was significantly elevated in the group receiving 450 mg/kg acetaminophen (Fig. 1F), whereas no differences in M2 macrophage ($CD45^+CD11b^+F4/80^+CD206^+$) composition were observed between treatment groups (Fig. 1G). Values recorded in the separately analysed right lobe were comparable and are provided in Table S3. Taken together, the data indicate that although serum markers of liver function were capable of distinguishing DILI following acetaminophen overdose, the values do not reflect

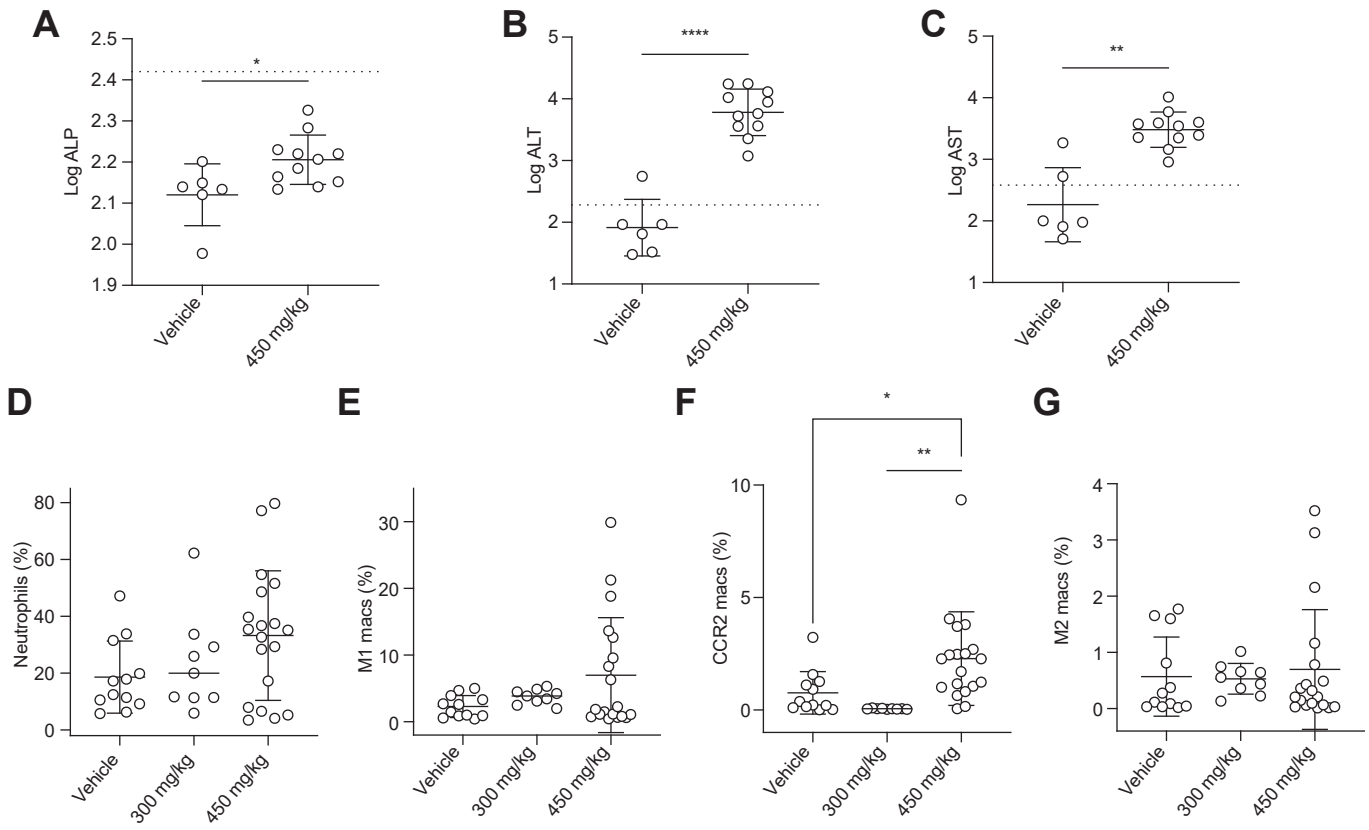

Fig. 1. Serum markers of liver function and intrahepatic myeloid cell content after treatment with either acetaminophen or vehicle. ALP (A), ALT (B), and AST (C) values plotted on log scale were elevated significantly in mice receiving 450 mg/kg compared with mice receiving vehicle. The dashed lines correspond to the normal upper limit. ALT levels were above thresholds consistent with DILI (ALT ≥ five times the normal upper limit) for all acetaminophen-treated mice, and beneath DILI thresholds for all vehicle-treated mice. (D–G) Flow cytometry assay indicates that the percentage of intrahepatic leucocytes comprised of neutrophils (D), M1 macrophages (E), CCR2 macrophages (F), and M2 macrophages (G) varies substantially within treatment groups. With the exception of elevated CCR2 macrophage content in mice receiving 450 mg/kg acetaminophen, intrahepatic myeloid cell content does not differ significantly between treatment groups. Statistics: data in (A–C) compared using the two-sided unpaired *t* test, data in (D–G) compared using one-way ANOVA followed by Tukey's *post-hoc* test for multiple comparisons. **p* <0.05, ***p* <0.005, ****p* <0.0005, *****p* <0.0001. ALP, alkaline phosphatase; ALT, alanine transaminase; AST, aspartate transaminase.

differences in liver inflammatory infiltrate composition. Liver test values correlated poorly with intrahepatic neutrophil composition (Table S4).

Liver signal enhancement at early time points following Fe-PyC3A injection correlates with intrahepatic neutrophil content

MR images recorded 2 min after Fe-PyC3A injection revealed differentially greater liver signal enhancement in mice where flow cytometry assay indicated higher levels of intrahepatic neutrophil content. The effect is illustrated by the representative coronal MR images of mice recorded before and 2 min after Fe-PyC3A injection shown in Fig. 2A–C, with corresponding H&E staining and flow cytometry dot plots showing Ly6G out of CD45 for liver tissue harvested from each mouse shown in the same rows. The images in Fig. 2A were acquired from a vehicle-treated mouse for which serum liver markers were found within the normal reference ranges, H&E staining indicated normal liver, and relatively low intrahepatic neutrophil content was recorded by flow cytometry. Note that Fe-PyC3A injection results in very little MR signal enhancement within the liver or in any adjacent tissue. The images in Fig. 2B correspond to an acetaminophen-treated mouse for which serum markers of hepatocellular damage were elevated to levels consistent with DILI[21] and H&E staining indicated substantial hepatocellular injury, but for which intrahepatic neutrophil levels remain relatively low. Here too, Fe-PyC3A generated little liver signal enhancement 2 min after injection. The images in Fig. 2C correspond to an acetaminophen-treated mouse with DILI confirmed by both serologic markers and histology and also exhibiting an acute inflammatory response evidenced by comparatively higher intrahepatic neutrophil content. Here, strong liver MR signal enhancement is observed 2 min after Fe-PyC3A injection. Although strong liver signal enhancement occurs, little signal enhancement is observed in the blood pool or adjacent muscle tissue, consistent with MR signal response that is specific to the inflamed liver tissue.

The (post-pre)injection liver *vs.* muscle contrast-to-noise ratio (ΔCNR) values recorded 2 min after injection (ΔCNR_{2m}) correlate positively and significantly (r = 0.64, p <0.0001) with intrahepatic neutrophil content (Fig. 1D and Table S5). The relative degree of liver signal enhancement 2 min after Fe-PyC3A appears to be weighted more heavily to the presence of neutrophils than any of the macrophage subpopulations analysed, which all correlated poorly with ΔCNR_{2m}.

The differential MR liver signal enhancement demonstrated in Fig. 2C is a largely transient effect, with liver signal decreasing rapidly after 2 min post-injection (Fig. S3).

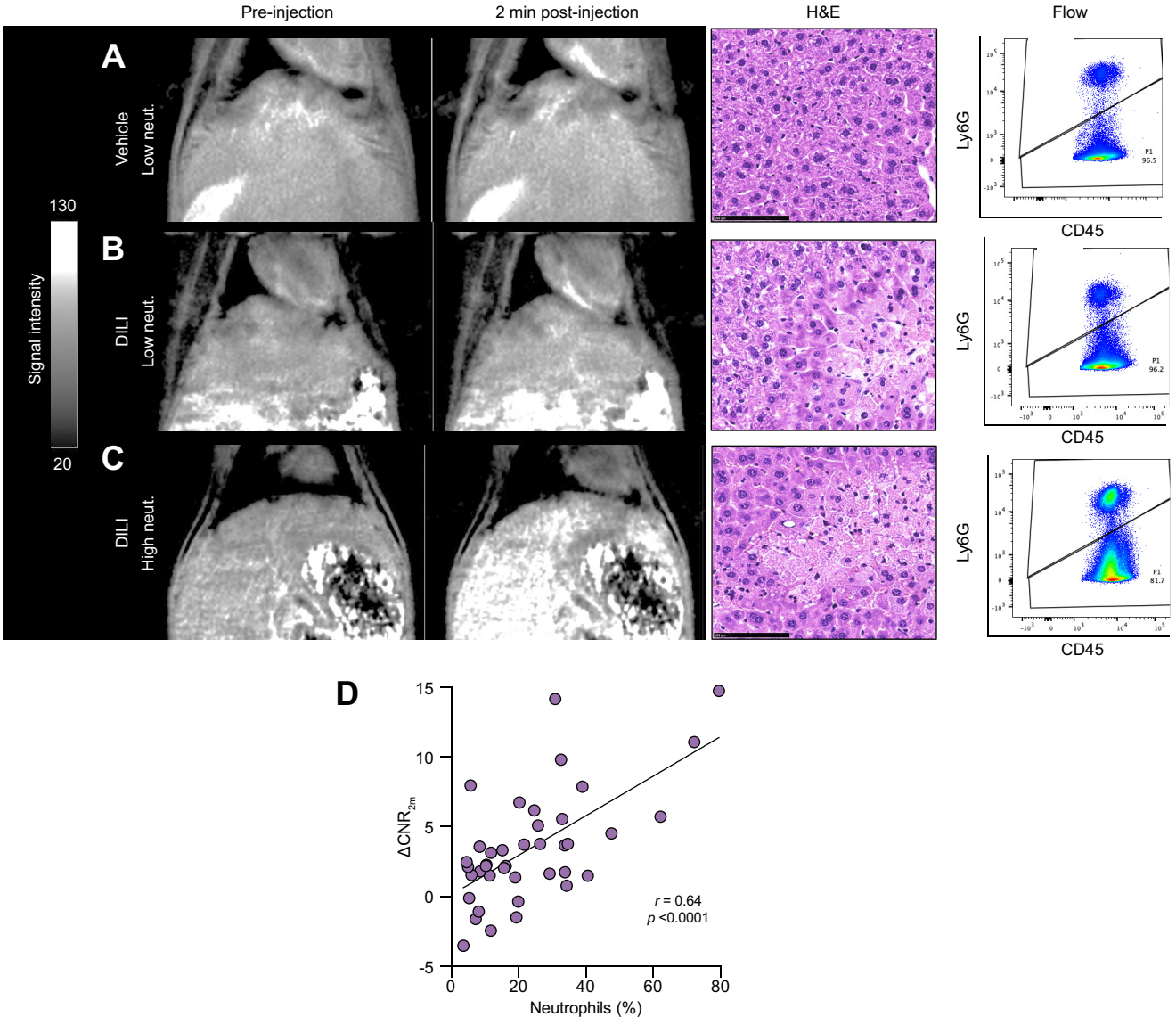

Fig. 2. Fe-PyC3A differentially generates MR signal enhancement in inflamed liver tissue. (A–C) Representative pre- and 2 min post-injection coronal T_1-weighted images, H&E staining, and flow cytometry dot plots showing Ly6G out of CD45 for mice receiving i.p. injections comprising vehicle (A) or hepatotoxic doses of acetaminophen (B, C). The acetaminophen treated mice have ALT levels consistent with DILI and hepatocellular injury is evidenced by H&E staining. Although both mice experience DILI, flow cytometry quantification of intrahepatic neutrophil composition indicates that only the mouse shown in (C) experiences an acute inflammatory response. Note how Fe-PyC3A generates little liver signal enhancement in the vehicle and acetaminophen treated mice exhibiting relatively low intrahepatic neutrophil composition (A and B), whereas strong liver signal enhancement is observed in the inflamed liver tissue of the acetaminophen treated mouse in (C). (D) Intrahepatic neutrophil composition recorded in the left liver lobe correlates positively and significantly with ΔCNR_{2m}. Statistics: correlation in (D) determined by calculating the Pearson's product moment correlation coefficient, significance was determined using a two-tailed test. ALT, alanine transaminase; CNR, contrast-to-noise ratio; DILI, drug-induced liver injury.

Molecular MR imaging of liver inflammation in a mouse model of NASH

We performed two experiments to investigate whether MR imaging using Fe-PyC3A was capable of detecting pathologic and inflammatory changes in a mouse model of NASH. To evaluate imaging with Fe-PyC3A as a potential proxy for histopathologic changes, we imaged mice receiving regimens of CDAHFD ranging between 2 and 13 days, and mice fed normal diet. For imaging comparisons, mice with NAS ≤3 and NAS ≥5 were grouped as likely non-NASH and likely NASH, respectively, based on criteria proposed by the NASH CRN.[16] The imaging data were also correlated with histologic scores and myeloperoxidase immunostaining. To evaluate whether MR imaging using Fe-PyC3A in steatotic liver was sensitive to changes in composition of intrahepatic myeloid cell sub-populations, we imaged mice fed 4-, 6-, and 8-week regimens of CDAHFD, and age-matched control mice fed normal diet. The mice were grouped for analysis according to differences in steatosis and intrahepatic myeloid cell content, and the imaging data correlated with neutrophil and macrophage subpopulation fractional composition determined via flow cytometry.

NASH can occur within 2 days of CDAHFD initiation and disease progresses faster in the right lobe

MRI and H&E staining demonstrated that pathologic changes associated with NASH occur within 2 days of CDAHFD initiation, and that disease progresses more rapidly in the right lobe of the liver as compared with the left lobe (Fig. 3). The axial T_2-weighted liver images (Fig. 3A) and corresponding protein density fat fraction (PDFF) maps generated from DIXON MRI (Fig. 3B and C) show how steatosis progresses from normal diet out to 13 days on CDAHFD, and demonstrate an overall greater accumulation of fat in the right liver lobe during this period. Histologic assessment (Fig. 3D and Fig. S4) of the right lobe confirmed NASH in two of the four mice imaged after only a 2-day regimen of CDAHFD, whereas specimens harvested from the left lobe received NAS ranging between 0 and 2. Taken together, imaging mice fed normal diet and mice on CDAHFD for periods ranging between 2 and 13 days enabled us to evaluate Fe-PyC3A imaging in mice receiving NAS scores ranging between 0 and 7 in the left lobe and 0 and 8 in the right lobe. Fibrosis stage ≤2 was determined for all liver specimens.

Liver myeloid cell content is expanded significantly in mice fed CDAHFD

H&E staining and Dixon MR imaging confirmed a high degree of steatosis in the CDAHFD-fed mice that did not change between 4 and 8 weeks on diet (Fig. S5). Myeloperoxidase immunostaining indicates that myeloperoxidase-positive cell content in mice fed 4- and 6-week regimens is roughly double that found in mice fed normal diet, and then again expands significantly between 6 and 8 weeks (Fig. 4A and B).

Flow cytometry analysis of left lobe leucocyte composition indicates that neutrophil fractional composition is modestly, but not significantly, increased in mice fed CDAHFD compared with normal diet, and does not change significantly between 4 and 8 weeks on CDAHFD (Fig. 4C and Table S6). Fractional composition comprising M1 and CCR2 macrophages recorded after 4 weeks on CDAHFD did not differ significantly from mice fed normal diet, but both M1 and CCR2 migratory macrophages increased significantly between 4 and 6 weeks, and then again between 6 and 8 weeks (Fig. 4D and E). After 4 and 6 weeks on the CDAHFD, fractional M2 macrophage composition did not differ from that

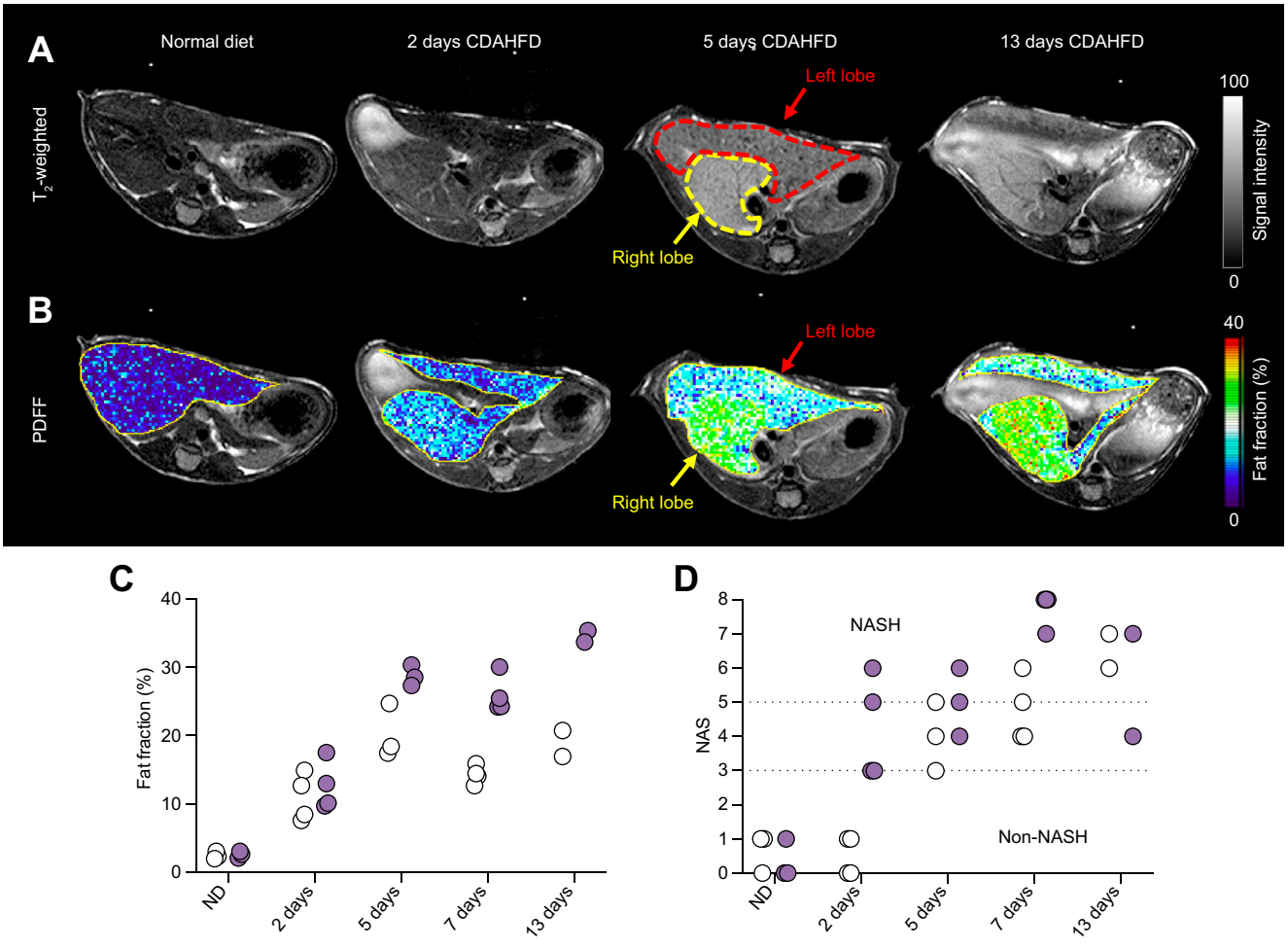

Fig. 3. Progression of NASH over 13 days on CDAHFD. (A, B) T_2-weighted images (A) and corresponding maps of proton density fat fraction (B) for mice receiving normal diet and on CDAHFD for 2 days, 5 days, or 13 days. (C, D) Fat fraction (C) and NAS (D) observed in the left lobe (filled circles) and right lobe (open circles) of mice receiving normal diet and varying periods of CDAHFD. The dotted lines at in (D) indicate the cut-offs for assignment of likely non-NASH (≤3) and likely NASH (≥5). CDAHFD, choline deficient, high-fat diet; NAS, NAFLD activity score; NASH, non-alcoholic steatohepatitis; PDFF, protein density fat fraction.

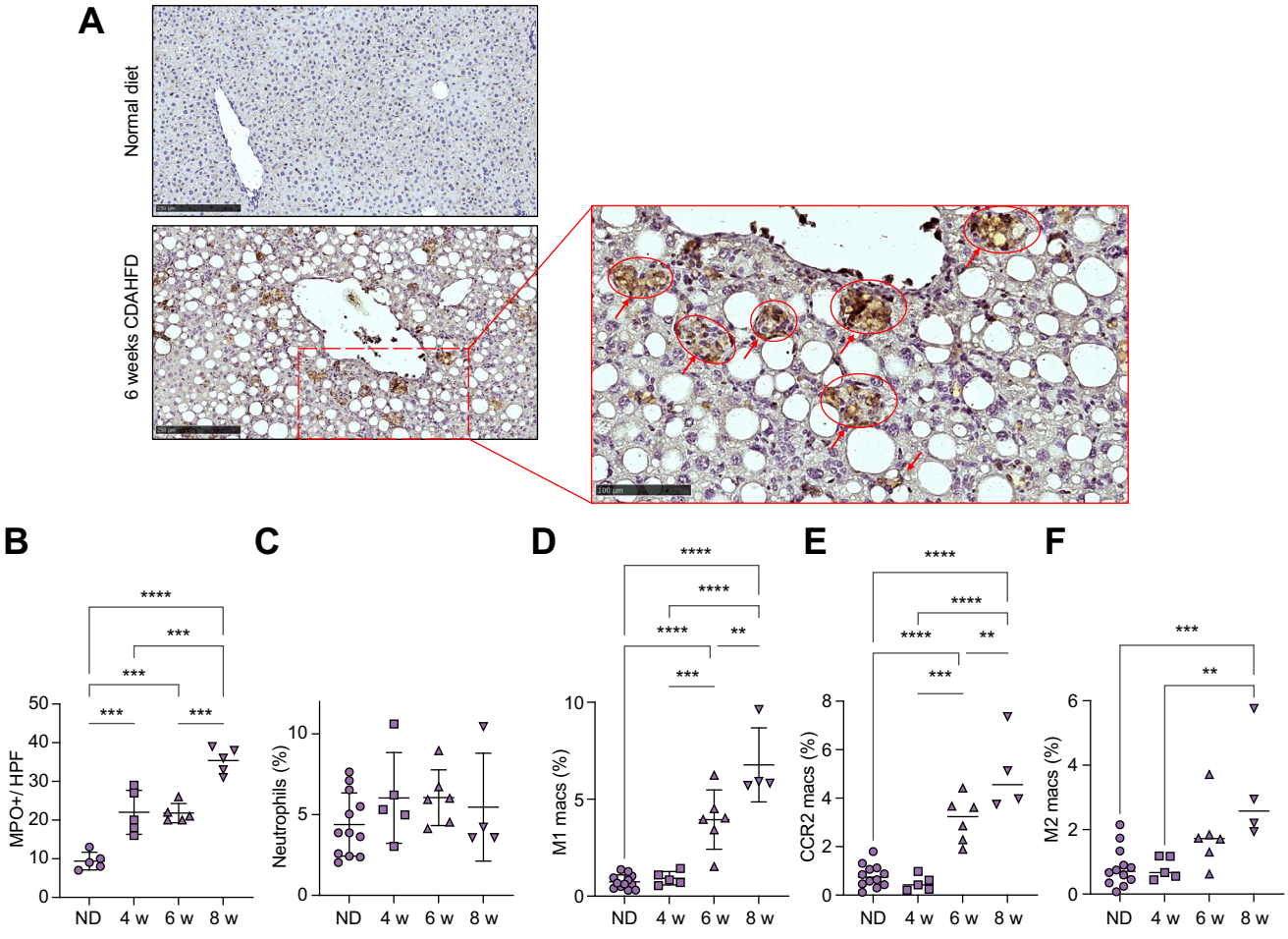

Fig. 4. *Ex vivo* quantitation of intrahepatic myeloid cell composition in mice fed CDAHFD and normal diet. (A) Myeloperoxidase immunostaining of tissue harvested from the left lobe of mice receiving normal diet or 6 weeks CDAHFD. (B–F) Comparisons of myeloperoxidase positive cell content (B) and percentage composition of intrahepatic neutrophils (C), M1 macrophages (D), CCR2 macrophages (E), and M2 macrophages (F) between groups of mice receiving normal diet and 4-, 6-, and 8-week regimens of CDAHFD. Statistics: data in (B–F) compared by one-way ANOVA followed by Tukey's *post-hoc* test for multiple comparisons. $^{*}p$ <0.05, $^{**}p$ <0.005, $^{***}p$ <0.0005, $^{****}p$ <0.0001. CDAHFD, choline deficient, high-fat diet; MPO, myeloperoxidase.

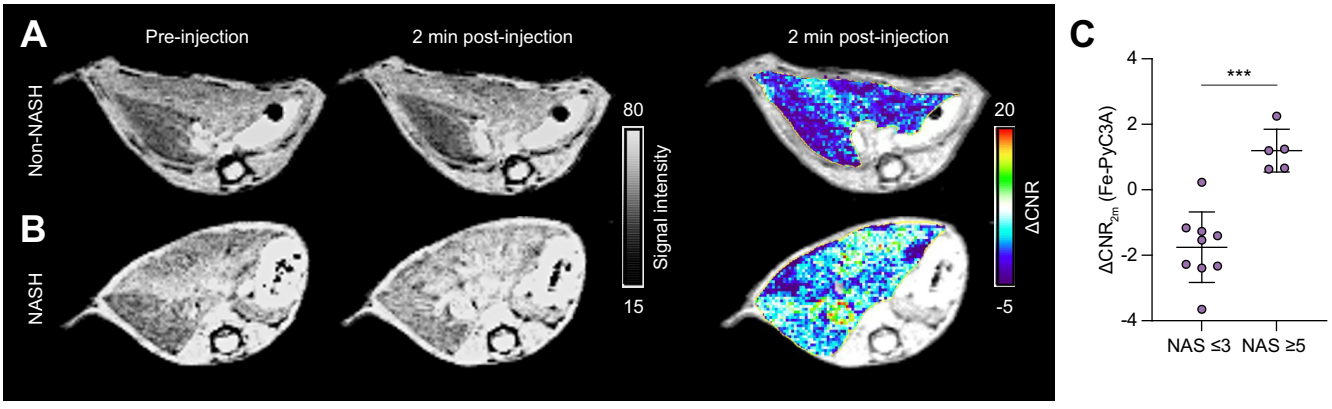

Fig. 5. Comparisons of MR imaging in likely non-NASH and likely NASH mice. (A, B) Comparison of axial T_1-weighted MR images of CDAHFD-fed mice receiving NAS scores consistent with likely non-NASH (A) and likely NASH (B) based on analysis of the left liver lobe. (C) Comparison of ΔCNR_{2m} values recorded in the left lobe of mice assigned as non-NASH and NASH. Statistics: data in (C) compared using a two-sided unpaired *t* test. $^{***}p$ = 0.001. CDAHFD, choline deficient, high-fat diet; CNR, contrast-to-noise ratio; NAS, NAFLD activity score; NASH, non-alcoholic steatohepatitis.

recorded in normal liver, but by 8 weeks increased significantly compared with normal liver and to liver after 4 weeks CDAHFD (Fig. 4F). Values recorded in the separately analysed right lobe were comparable and are provided in Table S7.

Fe-PyC3A distinguishes non-NASH *vs.* NASH in left liver lobe

Representative axial T_1-weighted images recorded before and 2 min after injection of Fe-PyC3A to mice receiving histologic scores consistent with NAS ≤3 (likely non-NASH) and NAS ≥5 (likely NASH) based on analysis of the liver left lobe are compared in Fig. 5A and B, respectively. Intravenous Fe-PyC3A injection generated very little liver signal enhancement in the mouse assigned to the likely non-NASH group whereas a modest degree of liver signal enhancement is observed in the mouse assigned to the likely NASH group. The ΔCNR_{2m} values recorded in the left liver lobe for mice designated as likely non-NASH and likely NASH based on histologic evaluation are compared in Fig. 5C, and demonstrate that left lobe enhancement is significantly greater (p = 0.0001) in mice assigned to the likely NASH group. The ΔCNR_{2m} values correlated positively and significantly with steatosis grade (r = 0.74, p = 0.0009) and hepatocellular ballooning (r = 0.69, p = 0.006), and tracked loosely but not significantly with inflammation grade (r = 0.45, p = 0.072) and myeloperoxidase positive cell content determined by immunohistochemistry (r = 0.48, p = 0.058). The time course of mean ΔCNR recorded in likely non-NASH and likely NASH mice are compared in Fig. S6, and demonstrate that the differential liver enhancement in NASH is transient and diminishes in magnitude by 4 min post-injection.

Left lobe MR signal enhancement after injection of the extracellular fluid MR imaging contrast agent Gd-DOTA did not distinguish between likely NASH and likely non-NASH (p = 0.92), The ΔCNR_{2m} values generated by Gd-DOTA are shown in Fig. S6, and the ΔCNR time course in Fig. S7. Left lobe enhancement after injection of Gd-DOTA also exhibited no correlation with any scoring component comprising NAS or with myeloperoxidase positive cell content (Table S8).

Interestingly, signal enhancement recorded in the right lobe of the liver did not differ significantly between likely non-NASH *vs.* likely NASH groups and did not correlate with any histologic score after injection with either Fe-PyC3A or Gd-DOTA (Table S9).

Fe-PyC3A MR signal enhancement in liver with advanced steatosis did not correlate definitively with any specific component of inflammatory infiltrate

Representative coronal abdominal T_1-weighted images recorded before and 2 min after injection of Fe-PyC3A to mice fed normal diet or a 6-week regimen of CDAHFD are compared in Fig. 6A and B, respectively, and demonstrated a greater degree of liver signal enhancement in the CDAHFD-fed mouse. The ΔCNR_{2m} values recorded for groups of mice receiving 4-, 6-, and 8-week regimens of CDAHFD are all significantly greater than for age-matched mice receiving normal diet (Fig. 6C). The differential enhancement observed in CDAHFD-fed mice reflects the overall increase in intrahepatic myeloperoxidase-positive cell content similar to that shown in Fig. 4. However, as time on diet progresses from 4 weeks to 8 weeks, the ΔCNR_{2m} values do not reflect relative differences in the flow cytometry data. For CDAHFD-fed mice, the ΔCNR_{2m} values did not correlate strongly or definitively with fractional composition of neutrophils or any macrophage sub-population (Table S10).

Discussion

Most acute and chronic liver disease states possess an inflammatory component. For example, inflammation is identified nearly invariantly on liver biopsy samples of patients suffering from DILI,[22] which is the most frequent form of drug-related

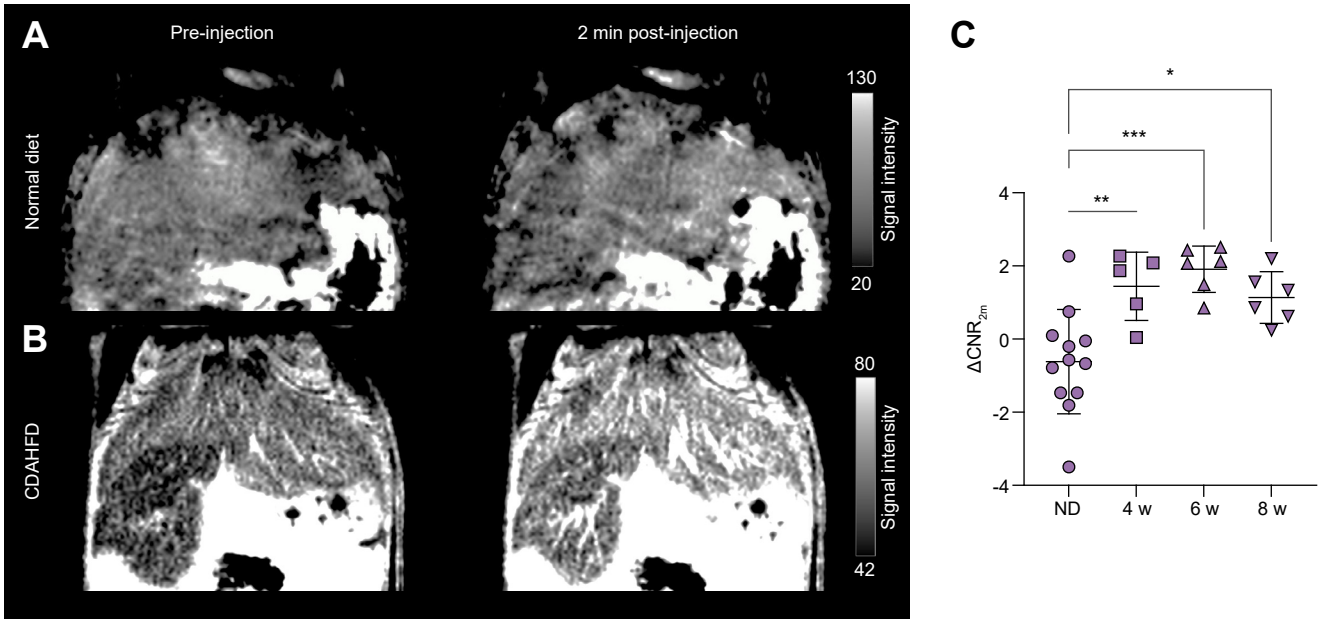

Fig. 6. MR imaging data recorded on mice fed normal diet and CDAHFD for between 4 and 8 weeks. (A, B) Comparison of coronal T_1-weighted MR images of mice fed normal diet (A) or a 6-week CDAHFD diet (B) recorded before and 2 min after i.v. injection of 0.2 mmol/kg Fe-PyC3A. (C) Comparison of ΔCNR_{2m} values recording in mice fed normal diet and 4-, 6-, and 8-week regimens of CDAHFD. Statistics: data in (C) compared using one-way ANOVA followed by Tukey's *post-hoc* test for multiple comparisons. *p <0.05, **p <0.01, ***p <0.001. CDAHFD, choline deficient, high-fat diet; CNR, contrast-to-noise ratio.

adverse event and a leading cause of acute liver failure.[21,23] Inflammation is also a key driver of chronic liver diseases.[2,3] Most major histologic scoring systems to diagnose or assess activity of chronic liver diseases, including scoring systems specific to viral hepatitis,[24–26] autoimmune hepatitis,[27,28] NAFLD,[16,29] alcohol-related liver disease,[16,30,31] and cholangitis[32,33] account for the presence of inflammation. Histologic assessment of inflammation often guides key decisions regarding patient management and therapeutic options. For example, inflammation is a key driver of NASH and an independent predictor for progression to advanced fibrosis.[34] For patients with chronic hepatitis B, decisions regarding the initiation of antiviral treatment are often based on the presence of liver inflammation.[35,36] Liver inflammation is also believed to lower thresholds for drug hepatotoxicity and may be weighed as a risk factor during therapeutic planning.[22,37]

Non-invasive biomarkers for liver inflammation are lacking. Serologic markers offer limited information regarding inflammation. Stiffness measurements using MR elastography and functional liver imaging using the hepatobiliary-specific MR imaging contrast agent gadoxetate are emerging as tools to image and stage fibrosis in advanced liver disease,[38–40] but imaging tools for inflammation are underdeveloped.[5] Non-invasive imaging of inflammation could offer substantial value in the context of chronic liver disease, as clinically significant progression and resolution of fibrosis occurs more slowly than changes in disease activity.[29] Multiparametric MR imaging including measurements of PDFF and MR elastography damping ratio is being experimentally evaluated as proxy for NAS.[41,42] Molecular imaging using probes targeted to specific cell- or molecular-level drivers of inflammation offers a potentially powerful non-invasive biomarker to detect, map, and quantify inflammation disease activity, but molecular imaging of liver inflammation faces specific challenges. For example, while nanoparticle-based MR imaging probes can be successfully applied to image infiltration of phagocytic immune cells in many organs,[6] the liver is an immunologic organ with a large population of resident macrophages, resulting in the confound of high non-specific background signal.[7,8] Similarly, small molecule positron emission tomography tracers like ^{18}F-fluorodeoxyglucose, which are commonly used to image macrophage activation, also accumulate in hepatocytes resulting in non-specific background signal.[9] Other studies have taken an opposite approach by demonstrating how steatosis-associated dysfunction of resident liver macrophages lessens liver accumulation of small and ultrasmall superparamagnetic iron-oxide particles and concomitant T_2^* shortening.[43] Liver uptake of ferumoxytol was shown to be significantly decreased in patients with NAS ≥5 compared with those with NAS ranging 2–3 or with normal liver.[44]

An alternate approach to imaging liver inflammation is to use low molecular weight imaging probes targeted to molecular markers located within the liver extracellular spaces. For example, delayed phase MR imaging using the myeloperoxidase-specific gadolinium-based probe Gd-MPO, which is polymerised and retained within the inflammatory microenvironment, was shown to distinguish NASH *vs.* simple steatosis in mice.[45] In another study, MR imaging of liver extravascular coagulation using the fibrin-specific and gadolinium-based MR imaging probe EP2104R was demonstrated as a potential marker of liver inflammation induced through exposure to diethylnitrosamine.[46]

We hypothesised that MR imaging using Fe-PyC3A could enable rapid visualisation, and potentially quantitation, of liver inflammation through detection of oxidative changes within the liver extracellular spaces resulting from myeloid cell respiratory burst activity. Based on prior detailed study of the pharmacokinetics of the isostructural compound Mn-PyC3A, which is being developed as an extracellular fluid MR imaging contrast agent,[17–20] intravenously injected Fe-PyC3A is expected to rapidly distribute through the extracellular fluid spaces and wash out within minutes through mixed renal (∼85%) and hepatobiliary (∼15%) excretion. Prior proof-of-concept imaging using a mouse model of pancreatitis showed that Fe-PyC3A generated strong MR signal enhancement of inflamed pancreatic tissue just minutes after injection followed by rapid signal washout consistent with expected extracellular distribution and rapid clearance. In that study, pancreatic MR signal enhancement was highly correlated with the presence of infiltrating myeloid cells determined via an *ex vivo* assay to quantify myeloperoxidase activity levels in pancreatic tissue.[11]

Our data indicate that Fe-PyC3A differentially generates positive MR signal enhancement in inflamed liver tissue. In the set of mice receiving either a hepatotoxic dose of acetaminophen or saline vehicle, the ΔCNR_{2m} values appears to trend with differences in intrahepatic neutrophil content that were not reflected in a panel of serologic markers commonly used to assess liver injury and to establish diagnosis of DILI in the clinical setting.[21] It is unclear why the inflammatory response varied so greatly in the acetaminophen group or why some animals in the group receiving vehicle exhibited a robust inflammatory response. We note that mean intrahepatic neutrophil content is substantially lower and the values less varied in the normal diet mice which did not receive i.p. injection of 500–750 μl vehicle. Nonetheless, the imaging data underscores how liver function tests lack specificity regarding liver inflammatory changes and highlights the potential power of MR imaging with Fe-PyC3A as a biomarker for liver inflammatory change.

MR imaging just 2 min after Fe-PyC3A injection was found to differentially generate MR liver signal enhancement in liver left lobe samples meeting histologic criteria consistent with NASH (NAS ≥5) that was significantly greater than in samples that were scored likely non-NASH (NAS ≤3). In contrast, liver enhancement observed using the extracellular fluid MRI contrast agent Gd-DOTA cannot distinguish NASH from likely non-NASH and correlated poorly with histologic measures of disease activity. Such findings further support the hypothesis that liver enhancement by Fe-PyC3A reflects oxidative changes rather than changes related to liver vascularisation and perfusion.

Amongst the myeloid cell populations assayed in our limited flow cytometry analysis, liver signal enhancement after Fe-PyC3A injection appears to have the strongest association with intrahepatic neutrophils, which are generally regarded as very potent ROS generators.[47] This is evidenced by the observation that early liver signal enhancement in DILI correlated most strongly with neutrophils. Similarly, the observation that early liver enhancement does not differ in mice on CDAHFD for between 4 and 8 weeks may be partially rationalised by the observation that neutrophil composition is largely unchanged within these groups. However, we note that the oxidising microenvironment is a functional property of inflamed tissue and the degree to which Fe-PyC3A activation occurs is likely dependent upon the degree of inflammatory cell infiltration, cell composition of the inflammatory infiltrate, as well as the respiratory burst activity of the various cell subpopulations. Further study is needed to more rigorously establish mechanistic links

between Fe-PyC3A liver signal generation and specific drivers contributing to the oxidising liver microenvironment.

Fe-PyC3A represents a novel molecular imaging technology that exhibits desirable features for potential imaging of liver inflammation in humans. As shown above, oxidatively driven switching from the low-relaxivity Fe^{2+} state to the high-relaxivity Fe^{3+} state minimises the non-specific background signal in normal tissues while generating positive MR signal in inflamed liver tissue in T_1-weighted MRI acquisitions similar to those routinely used in clinical practice. Comparisons of liver signal enhancement to reference tissue such as muscle may enable quantitation of inflammatory disease activity, analogous to how ΔCNR values were shown above to reflect intrahepatic neutrophil content in DILI and to correlate with NAS. The rapid Fe-PyC3A signal response is also advantageous for clinical imaging. Most molecularly targeted MR imaging probes and radiotracers generate a non-specific signal, and thus require a long delay between injection and imaging to allow for washout of the unbound probe. However, the near instantaneous oxidatively mediated response of Fe-PyC3A would enable imaging that is compatible with currently established high-throughput radiologic workflows. Another potentially attractive feature of Fe-PyC3A is that it utilises iron, rather than gadolinium, as the MR signal generating component. Gadolinium-based MR imaging probes have come under increasing regulatory scrutiny over concerns of toxicity related to residually retained gadolinium.[48–50] Iron however, is a nutritional element present in gram quantities in human adults.

There are some limitations to the study. Our study was designed to evaluate MR imaging using Fe-PyC3A in the context of intrahepatic myeloid cell content, but it did not include measurements to assess non-immunologic sources of intrahepatic ROS that may also contribute to Fe-PyC3A oxidation and liver signal increase. For example, acetaminophen hepatotoxicity arises from both depletion of hepatocyte anti-oxidant defence mechanisms and disruption of the mitochondria electron transport chain resulting in hepatocellular oxidative stress.[51] Given the expected partial hepatobiliary clearance of Fe-PyC3A,[11,17–20] probe oxidation by ROS present within oxidatively stressed hepatocytes may not be ruled out as a driver of liver signal enhancement. We also note that although our flow cytometry assay provided information on fractional composition of myeloid cell subpopulations out of leucocytes, the data do not inform on relative differences in absolute quantity. Another limitation is that ROS generating myeloid cells represents only one facet of the nuanced cellular determinants of liver inflammation. For example, immune cells of lymphoid origin such as cytotoxic T-cells, although not typically associated with ROS generation are also key drivers of disease activity in inflammatory liver conditions. The observation that Fe-PyC3A liver enhancement tracked only loosely with lobular inflammation and with myeloperoxidase immunostaining may partially reflect this limitation. Finally, it is important to note that although imaging using Fe-PyC3A was shown to distinguish likely NASH *vs.* likely non-NASH in the liver left lobe, the imaging failed to distinguish likely NASH *vs.* likely non-NASH in the right lobe. It is presently unclear why Fe-PyC3A performance is not consistent across different sections of the liver. We do note that for specimens where imaging was correlated with histology, more severe steatosis was observed in the right lobe. Prior studies have demonstrated that increasing steatosis blunts the magnitude of liver signal enhancement following contrast agent injection.[52] A limitation of this work is that we did not examine increased fat fraction as a potential confounding factor for our imaging.

The results of our study preliminarily indicate that the oxidatively activated MR imaging probe Fe-PyC3A generates liver signal differentially within the oxidising inflammatory liver microenvironment. The results indicate that MR imaging using oxidatively activated iron-based MR imaging probes such as Fe-PyC3A, or future optimised iterations of this technology, warrants further evaluation and development for non-invasive imaging of liver inflammation.

Abbreviations

ALP, alkaline phosphatase; ALT, alanine transaminase; AST, aspartate transaminase; CDAHFD, choline deficient, high-fat diet; CNR, contrast-to-noise ratio; CRN, Clinical Research Network; DILI, drug-induced liver injury; Fe^{2+}, divalent iron; Fe^{3+}, trivalent iron; Gd-DOTA, gadoterate meglumine; H&E, haematoxylin and eosin stain; MGE, multiple gradient echo; MR, magnetic resonance; NAFLD, non-alcoholic fatty liver disease; NAS, NAFLD activity score; NASH, non-alcoholic steatohepatitis; PDFF, protein density fat fraction; ROI, regions of interest; ROS, reactive oxygen species; SI, signal intensity; TE, echo time; TR, repetition time.

Financial support

This work was supported by grants from the National Institute of Diabetes and Digestive and Kidney Diseases (R01DK120663, R01DK121789, R01DK108370), the National Institute of Allergy and Infectious Diseases (R01AI136715), the National Heart, Lung, and Blood Institute (K25HL128899), the NIH Office of the Director (S10OD032138, S10OD025234), the MGH Research Scholars Program, and a sponsored research agreement with Bristol Meyers Squibb.

Conflicts of interest

EMG holds equity in, and receives consulting income from Reveal Pharmaceuticals, and receives consulting income from Collagen Medical, LLC. PC holds equity in, and receives consulting income from Collagen Medical LLC, holds equity in Reveal Pharmaceuticals, and has research funding from Takeda, Pliant Therapeutics, and Janssen.

Please refer to the accompanying ICMJE disclosure forms for further details.

Authors' contributions

Study design: VCJ, MS, JW, PC, EMG. Data analysis: VCJ, MS, PC, EMG. MRI data acquisition: VCJ, EMG. MRI data processing: VCJ, PGP. Flow cytometry, histology, and immunohistochemistry: MS, PGP, SCB. Blinded pathology review: SS. Manuscript preparation and review: VCJ, MS, JW, KKT, RTC, PC, EMG.

Data availability statement

Data generated through these studies are available from the corresponding author on reasonable request.

Supplementary data

Supplementary data to this article can be found online at https://doi.org/10.1016/j.jhepr.2023.100850.

References

Author names in bold denote co-first authorship

[1] **Asrani SK**, **Devarbhavi H**, Eaton J, Kamath PS. Burden of liver diseases in the world. J Hepatol 2019;70:151–171.
[2] Koyama Y, Brenner DA. Liver inflammation and fibrosis. J Clin Invest 2017;127:55–64.

[3] Del Campo JA, Gallego P, Grande L. Role of inflammatory response in liver diseases: therapeutic strategies. World J Hepatol 2018;10:1–7.
[4] Ros PR. Imaging of diffuse and inflammatory liver disease. In: Hodler J, Kubik-Huch RA, von Schulthess GK, editors. Diseases of the abdomen and pelvis 2018–2021: diagnostic imaging – IDKD book; 2018. p. 237–246. Cham (CH).
[5] Jayakumar S, Harrison SA, Loomba R. Noninvasive markers of fibrosis and inflammation in nonalcoholic fatty liver disease. Curr Hepatol Rep 2016;15:86–95.
[6] Neuwelt A, Sidhu N, Hu CAA, Mlady G, Eberhardt SC, Sillerud LO. Iron-based superparamagnetic nanoparticle contrast agents for MRI of infection and inflammation. Am J Roentgenol 2015;204:W302–W313.
[7] Li S-D, Huang L. Pharmacokinetics and biodistribution of nanoparticles. Mol Pharmaceutics 2008;5:496–504.
[8] Reimer P, Balzer T. Ferucarbotran (Resovist): a new clinically approved RES-specific contrast agent for contrast-enhanced MRI of the liver: properties, clinical development, and applications. Eur Radiol 2003;13:1266–1276.
[9] Keramida G, Potts J, Bush J, Verma S, Dizdarevic S, Peters AM. Accumulation of (18)F-FDG in the liver in hepatic steatosis. Am J Roentgenol 2014;203:643–648.
[10] Jiang JX, Torok NJ. NADPH oxidases in chronic liver diseases. Adv Hepatol 2014;2014:742931.
[11] **Wang H**, **Clavijo Jordan V**, **Ramsay IA**, Sojoodi M, Fuchs BC, Tanabe KK, et al. Molecular magnetic resonance imaging using a redox-active iron complex. J Am Chem Soc 2019;141:5916–5925.
[12] Percie du Sert N, Ahluwalia A, Alam S, Avey MT, Baker M, Browne WJ, et al. Reporting animal research: explanation and elaboration for the ARRIVE guidelines 2.0. Plos Biol 2020;18:e3000411.
[13] Matsumoto M, Hada N, Sakamaki Y, Uno A, Shiga T, Tanaka C, et al. An improved mouse model that rapidly develops fibrosis in non-alcoholic steatohepatitis. Int J Exp Pathol 2013;94:93–103.
[14] Reeder SB, Wen Z, Yu H, Pineda AR, Gold GE, Markl M, et al. Multicoil Dixon chemical species separation with an iterative least-squares estimation method. Magn Reson Med 2004;51:35–45.
[15] Yu H, Shimakawa A, McKenzie CA, Brodsky E, Brittain JH, Reeder SB. Multiecho water-fat separation and simultaneous R2* estimation with multifrequency fat spectrum modeling. Magn Reson Med 2008;60:1122–1134.
[16] Kleiner DE, Brunt EM, Van Natta M, Behling C, Contos MJ, Cummings OW, et al. Design and validation of a histological scoring system for nonalcoholic fatty liver disease. Hepatology 2005;41:1313–1321.
[17] Zhou IY, Ramsay IA, Ay I, Pantazopoulos P, Rotile NJ, Wong A, et al. Positron emission tomography-magnetic resonance imaging pharmacokinetics, in vivo biodistribution, and whole-body elimination of Mn-PyC3A. Invest Radiol 2021;56:261–270.
[18] Erstad DJ, Ramsay IA, Jordan VC, Sojoodi M, Fuchs BC, Tanabe KK, et al. Tumor contrast enhancement and whole-body elimination of the manganese-based magnetic resonance imaging contrast agent Mn-PyC3A. Invest Radiol 2019;54:697–703.
[19] Gale EM, Wey HY, Ramsay I, Yen YF, Sosnovik D, Caravan P. A manganese-based alternative to gadolinium: contrast enhanced MR angiography, pharmacokinetics, and metabolism. Radiology 2018;286:865–872.
[20] Gale EM, Atanasova I, Blasi F, Ay I, Caravan P. A manganese alternative to gadolinium for MRI contrast. J Am Chem Soc 2015;137:15548–15557.
[21] European Association for the Study of the Liver. EASL clinical practice guidelines: drug-induced liver injury. J Hepatol 2019;70:1222–1261.
[22] Roth RA, Ganey PE. Drug-induced liver disease. In: Kaplowitz N, DeLeve LD, editors. Drug-induced liver disease. 3rd ed. Amsterdam: Elsevier; 2013. p. 157–172.
[23] David S, Hamilton JP. Drug-induced liver injury. US Gastroenterol Hepatol Rev 2010;6:73–80.
[24] Knodell RG, Ishak KG, Black WC, Chen TS, Craig R, Kaplowitz N, et al. Formulation and application of a numerical scoring system for assessing histological activity in asymptomatic chronic active hepatitis. Hepatology 1981;1:431–435.
[25] Bedossa P, Poynard T. An algorithm for the grading of activity in chronic hepatitis C. The METAVIR Cooperative Study Group. Hepatology 1996;24:289–293.
[26] Ishak K, Baptista A, Bianchi L, Callea F, De Groote J, Gudat F, et al. Histological grading and staging of chronic hepatitis. J Hepatol 1995;22:696–699.
[27] Hennes EM, Zeniya M, Czaja AJ, Pares A, Dalekos GN, Krawitt EL, et al. Simplified criteria for the diagnosis of autoimmune hepatitis. Hepatology 2008;48:169–176.
[28] Balitzer D, Shafizadeh N, Peters MG, Ferrell LD, Alshak N, Kakar S. Autoimmune hepatitis: review of histologic features included in the simplified criteria proposed by the international autoimmune hepatitis group and proposal for new histologic criteria. Mod Pathol 2017;30:773–783.
[29] Sanyal AJ, Brunt EM, Kleiner DE, Kowdley KV, Chalasani N, Lavine JE, et al. Endpoints and clinical trial design for nonalcoholic steatohepatitis. Hepatology 2011;54:344–353.
[30] Elphick DA, Dube AK, McFarlane E, Jones J, Gleeson D. Spectrum of liver histology in presumed decompensated alcoholic liver disease. Am J Gastroenterol 2007;102:780–788.
[31] **Lackner C**, **Stauber RE**, Davies S, Denk H, Dienes HP, Gnemmi V, et al. Development and prognostic relevance of a histologic grading and staging system for alcohol-related liver disease. J Hepatol 2021;75:810–819.
[32] Portmann B, Zen Y. Inflammatory disease of the bile ducts-cholangiopathies: liver biopsy challenge and clinicopathological correlation. Histopathology 2012;60:236–248.
[33] **de Vries EM**, **de Krijger M**, Farkkila M, Arola J, Schirmacher P, Gotthardt D, et al. Validation of the prognostic value of histologic scoring systems in primary sclerosing cholangitis: an international cohort study. Hepatology 2017;65:907–909.
[34] Argo CK, Northup PG, Al-Osaimi AM, Caldwell SH. Systematic review of risk factors for fibrosis progression in non-alcoholic steatohepatitis. J Hepatol 2009;51:371–379.
[35] Sarin SK, Kumar M, Lau GK, Abbas Z, Chan HL, Chen CJ, et al. Asian-Pacific clinical practice guidelines on the management of hepatitis B: a 2015 update. Hepatol Int 2016;10:1–98.
[36] European Association for the Study of the Liver. EASL 2017 Clinical Practice Guidelines on the management of hepatitis B virus infection. J Hepatol 2017;67:370–398.
[37] Hoppmann NA, Gray ME, McGuire BM. Drug-induced liver injury in the setting of chronic liver disease. Clin Liver Dis 2020;24:89–106.
[38] Younossi ZM, Loomba R, Anstee QM, Rinella ME, Bugianesi E, Marchesini G, et al. Diagnostic modalities for nonalcoholic fatty liver disease, nonalcoholic steatohepatitis, and associated fibrosis. Hepatology 2018;68:349–360.
[39] Imajo K, Kessoku T, Honda Y, Tomeno W, Ogawa Y, Mawatari H, et al. Magnetic resonance imaging more accurately classifies steatosis and fibrosis in patients with nonalcoholic fatty liver disease than transient elastography. Gastroenterology 2016;150:626–637.e7.
[40] **Bastati N**, **Beer L**, Mandorfer M, Poetter-Lang S, Tamandl D, Bican Y, et al. Does the functional liver imaging score derived from gadoxetic acid-enhanced MRI predict outcomes in chronic liver disease? Radiology 2020;294:98–107.
[41] Allen AM, Shah VH, Therneau TM, Venkatesh SK, Mounajjed T, Larson JJ, et al. The role of three-dimensional magnetic resonance elastography in the diagnosis of nonalcoholic steatohepatitis in obese patients undergoing bariatric surgery. Hepatology 2020;71:510–521.
[42] Allen AM, Shah VH, Therneau TM, Venkatesh SK, Mounajjed T, Larson JJ, et al. Multiparametric magnetic resonance elastography improves the detection of NASH regression following bariatric surgery. Hepatol Commun 2020;4:185–192.
[43] Asanuma T, Ono M, Kubota K, Hirose A, Hayashi Y, Saibara T, et al. Super paramagnetic iron oxide MRI shows defective Kupffer cell uptake function in non-alcoholic fatty liver disease. Gut 2010;59:258–266.
[44] Smits LP, Coolen BF, Panno MD, Runge JH, Nijhof WH, Verheij J, et al. Noninvasive differentiation between hepatic steatosis and steatohepatitis with MR imaging enhanced with USPIOs in patients with nonalcoholic fatty liver disease: a proof-of-concept study. Radiology 2016;278:782–791.
[45] Pulli B, Wojtkiewicz G, Iwamoto Y, Ali M, Zeller MW, Bure L, et al. Molecular MR imaging of myeloperoxidase distinguishes steatosis from steatohepatitis in nonalcoholic fatty liver disease. Radiology 2017;284:390–400.
[46] Atanasova I, Sojoodi M, Leitao HS, Shuvaev S, Geraldes C, Masia R, et al. Molecular magnetic resonance imaging of fibrin deposition in the liver as an indicator of tissue injury and inflammation. Invest Radiol 2020;55:209–216.
[47] Forman HJ, Torres M. Reactive oxygen species and cell signaling: respiratory burst in macrophage signaling. Am J Respir Crit Care Med 2002;166:S4–S8.
[48] Marckmann P, Skov L, Rossen K, Dupont A, Damholt MB, Heaf JG, et al. Nephrogenic systemic fibrosis: suspected causative role of gadodiamide used for contrast-enhanced magnetic resonance imaging. J Am Soc Nephrol 2006;17:2359–2362.
[49] Kanda T, Fukusato T, Matsuda M, Toyoda K, Oba H, Kotoku J, et al. Gadolinium-based contrast agent accumulates in the brain even in subjects

without severe renal dysfunction: evaluation of autopsy brain specimens with inductively coupled plasma mass spectroscopy. Radiology 2015;276:228–232.
[50] McDonald RJ, Weinreb JC, Davenport MS. Symptoms associated with gadolinium exposure (SAGE): a suggested term. Radiology 2022;302:270–273.
[51] Ramachandran A, Jaeschke H. Mechanisms of acetaminophen hepatotoxicity and their translation to the human pathophysiology. J Clin Transl Res 2017;3:157–169.
[52] Pirasteh A, Clark HR, Sorra EA 2nd, Pedrosa I, Yokoo T. Effect of steatosis on liver signal and enhancement on multiphasic contrast-enhanced magnetic resonance imaging. Abdom Radiol (NY) 2016;41:1744–1750.